Meteorologische Zeitschrift, PrePub DOI 10.1127/metz/2016/0661

Representation of the Antarctic Oscillation and related precipitation patterns in the MPI Earth System Model

Stella Babian*, Henning W. Rust, Jens Grieger, Kerstin Prömmel and Ulrich Cubasch

Meteorological Institute, Freie Universität Berlin, Germany

(Manuscript received December 16, 2014; in revised form September 7, 2015; accepted August 10, 2016)

Abstract

The Antarctic Oscillation (AAO) is the dominant mode of atmospheric variability in the southern hemisphere. It is obtained via a principal component analysis (PCA) for geopotential height anomalies. Being the southern hemisphere's dominant mode, an adequate representation in earth system models is desirable. This paper evaluates to what extent the AAO and related precipitation is represented in the Max Planck Institute's Earth System Model (MPI-ESM). To this end we compare AAO spatial patterns (empirical orthogonal functions, EOFs), spectral properties of the associated principal components (PCs) and AAO-related precipitation patterns of MPI-ESM to three reanalyses: the ECMWF's ERA-40 and ERA-Interim, and the NCEP/NCAR 40-year reanalysis project. Differences between MPI-ESM and ERA-Interim leading EOFs reveal that the three typical centres of action are less pronounced and slightly shifted in the model. Spectral density estimates of the associated PCs show reduced variability in the MPI-ESM for periods between 4 to 5 months. The relation between AAO and southern hemispheric precipitation is assessed via composites and correlation analysis. In both, model and reanalyses, a negative AAO index leads to a general increase of precipitation between 30° S and 50° S and a decrease south of 50° S. Differences between maps of correlation for AAO and precipitation are most prominent near Indonesia and Antarctica probably due to a lack of pressure around Antarctica in the model. Altogether the MPI-ESM underestimates the relation of AAO and southern hemispheric precipitation but gives the correct sign and spatial distribution of correlation values.

Keywords: Antarctic Oscillation, MPI-ESM-MR, precipitation, southern hemisphere

1 Introduction

The most important pattern of climate variability in the southern hemisphere middle and high latitudes is the Southern Annular Mode (SAM). This variability mode is defined as the leading empirical orthogonal function (EOF) of the 700 hPa geopotential height anomaly field south of 20° S (Thompson and Wallace, 2000; Mo, 2000). The SAM is also referred to as Antarctic Oscillation (AAO). The predominant pattern (leading EOF) of the AAO is roughly circular with its centre at the south pole (zonally symmetric) and changes sign between 40° S to 50° S (Thompson and Wallace, 2000; Kidson, 1999; Climate Prediction Center, 2014). Phases with a positive AAO index are by convention associated with positive geopotential height anomalies over the midlatitudes and negative anomalies over Antarctica; vice versa for negative phases. The temporally evolving meridional geopotential height gradient results in periodical strengthening and weakening of the circumpolar vortex in the southern hemisphere which, in turn, affects other meteorological fields.

As the leading mode of temporal variability of atmospheric circulation in the southern hemisphere, the AAO has remarkable impacts on regional climate (Rashid and Simmonds, 2005). Several studies examined selected climatological parameters with respect to potential connections with the AAO: changes in strength and location of the westerlies (Kidson, 1988), stormtracks and extratropical cyclones (Pezza et al., 2008), connections to air temperatures in Antarctica (van den Broeke and van Lipzig, 2004), sea surface temperatures in the southern oceans (Mo, 2000), and temperature and precipitation over southern South America (Silvestri and Vera, 2003; Moy et al., 2009; Carvalho et al., 2005; Berman et al., 2012; Berman et al., 2013; Silvestri and Vera, 2009), western South Africa (Reason and Rouault, 2005; Gillett et al., 2006), and New-Zealand-Australia (Renwick and Thompson, 2006; Ummenhofer and England, 2007; Meneghini et al., 2007) were established.

Given the importance of the AAO for the southern hemisphere, an adequate representation in a climate model is highly desirable. Here, we assess the Max-Planck-Institute's Earth System Model (Giorgetta et al., 2013) for its potential to represent the AAO and related precipitation patterns. Primary aim of this study is thus to contribute an new important aspect to the validation of the MPI-ESM. The MPI-ESM participated in the 5th Coupled Model Intercomparison Project (CMIP5 Taylor et al., 2012) for climate projections and for the associated decadal prediction experiments. The latter has been part of CMIP for the first time in CMIP5.

*Corresponding author: Stella Babian, Meteorological Institute, Freie Universität Berlin, Carl-Heinrich-Becker-Weg 6–10, 12165 Berlin, Germany, e-mail: stella.babian@met.fu-berlin.de

The MPI-ESM is also the basis of the German national initiative for decadal prediction (MiKlip, *Mittelfristige Klimaprognose*) (Marotzke et al., 2016; Müller et al., 2012; Pohlmann et al., 2013; Kruschke et al., 2014, and all articles in this issue) [1].

This work compares the AAO spatial pattern (EOFs), the spectral properties of the associated PCs, and AAO-related precipitation patterns as found in the MPI-ESM to three reanalysis data sets: the European Centre for Medium Range Weather Forecast's 40-year (Uppala et al., 2005) and ERA-Interim reanalysis projects (Dee et al., 2011), as well as the National Center for Environmental Prediction and National Center for Atmospheric Research 40-year reanalysis project (Kalnay et al., 1996; Kistler et al., 2001).

Details on model simulations and reanalysis data sets used, as well as aspects of employed techniques are given in Section 2. Section 3 compares the spatial patterns of the AAO, discusses characteristics of the spectral properties of the related index time series and investigates the link between the model/reanalyses AAO index time series and southern hemispheric precipitation. A summary and discussion of the results is given in Section 4.

2 Data and methods

2.1 MPI-ESM Earth System Model

Various initialisation techniques have been used to perform decadal prediction experiments (Müller et al., 2012; Pohlmann et al., 2013; Kruschke et al., 2016) with the Max-Planck-Institute's Earth System Model (Giorgetta et al., 2013). The MPI-ESM consists of an atmospheric component, ECHAM6 (Stevens et al., 2013), an ocean and sea ice model MPIOM (Marsland et al., 2003; Giorgetta et al., 2013) coupled with OASIS3 (Valcke, 2013). Furthermore, the subsystems JSBACH (Raddatz et al., 2007) and HAMOCC (Ilyina et al., 2013) contribute the biosphere and the biogeochemical processes.

Here, we consider the MPI-ESM-MR (mixed resolution) with a T63 resolution in the atmosphere, similar to the LR (low resolution) version of the MPI-ESM but with an extended vertical resolution of 95 levels (instead of 47 levels in LR) reaching up to 0.01 hPa. The horizontal resolution corresponds to a $1.88° \times 1.88°$ grid. The oceanic component of the model is available on a $0.4° \times 0.4°$ grid and 40 vertical levels (Marotzke et al., 2016).

We use a so-called historical run (MPI-ESM-MR-hist) with the radiative forcing (boundary conditions) given by the observed forcing for the period from 1850 to 2005 and an interactive carbon cycle. These uninitialised historical runs of the particular model with prescribed boundary conditions serve as reference experiments within MiKlip to quantify predictive power (skill) of initialised over uninitialised runs.

[1] See also http://www.fona-miklip.de/en/index.php

Table 1: Resolution, levels and available time periods of NCEP/NCAR, ERA-Interim, ERA-40, and of the historical run of the MPI-ESM. The resulting common period of reanalyses and model run is 1979–2001.

Model/Data time period available	horizontal resolution	vertical levels
NCEP/NCAR 1948–2005	2.5°	17
ERA-40 1958–2001	3.75°	23
ERA-Interim 1979–2013	1.5°	37
MPI-ESM (Atm./Ocean)	1.88°(T63)/0.4°	

2.2 Reanalyses

Three reanalyses datasets provide the reference for this study: the National Center for Environmental Prediction and National Center for Atmospheric Research (NCEP/NCAR) reanalysis (Kalnay et al., 1996; Kistler et al., 2001), the ERA-40 (Uppala et al., 2005), and ERA-Interim (Dee et al., 2011) reanalysis data from the European Centre for Medium Range Weather Forecast (ECMWF). Table 1 gives further details on the three reanalysis datasets and the MPI-ESM.

The monthly mean geopotential height at 700 hPa (Z_{700}) is the basis for defining the AAO pattern and index. The monthly precipitation rate from NCEP/NCAR and the monthly total precipitation sums from the ECMWF products ERA-40 and ERA-Interim provide reliable precipitation data for the southern hemisphere.

2.3 Definition of the Antarctic Oscillation Index

The first EOF of a principal component analysis (Jolliffe, 2002; Hannachi et al., 2007) of the monthly mean Z_{700} anomalies south of 20° S over the southern hemisphere defines the spatial pattern of the AAO (Thompson and Wallace, 2000; Mo, 2000; Climate Prediction Center, 2014); the associated principal component (PC) the AAO index time series. The geopotential height anomalies are taken with respect to a mean annual cycle obtained by averaging individual month of the year for the period 1979–2001. The individual grid cells are centred and scaled with the square-root of their latitude to account for different grid cell sizes.

2.4 Spectral analysis

A spectral analysis of the principal components reveals their activity on various time scales. The classical Fourier periodogram is obtained from the index time series, tapered with a split cosine for 10 % of the data at both ends. An associated consistent estimate of the spectral density can be obtained in two

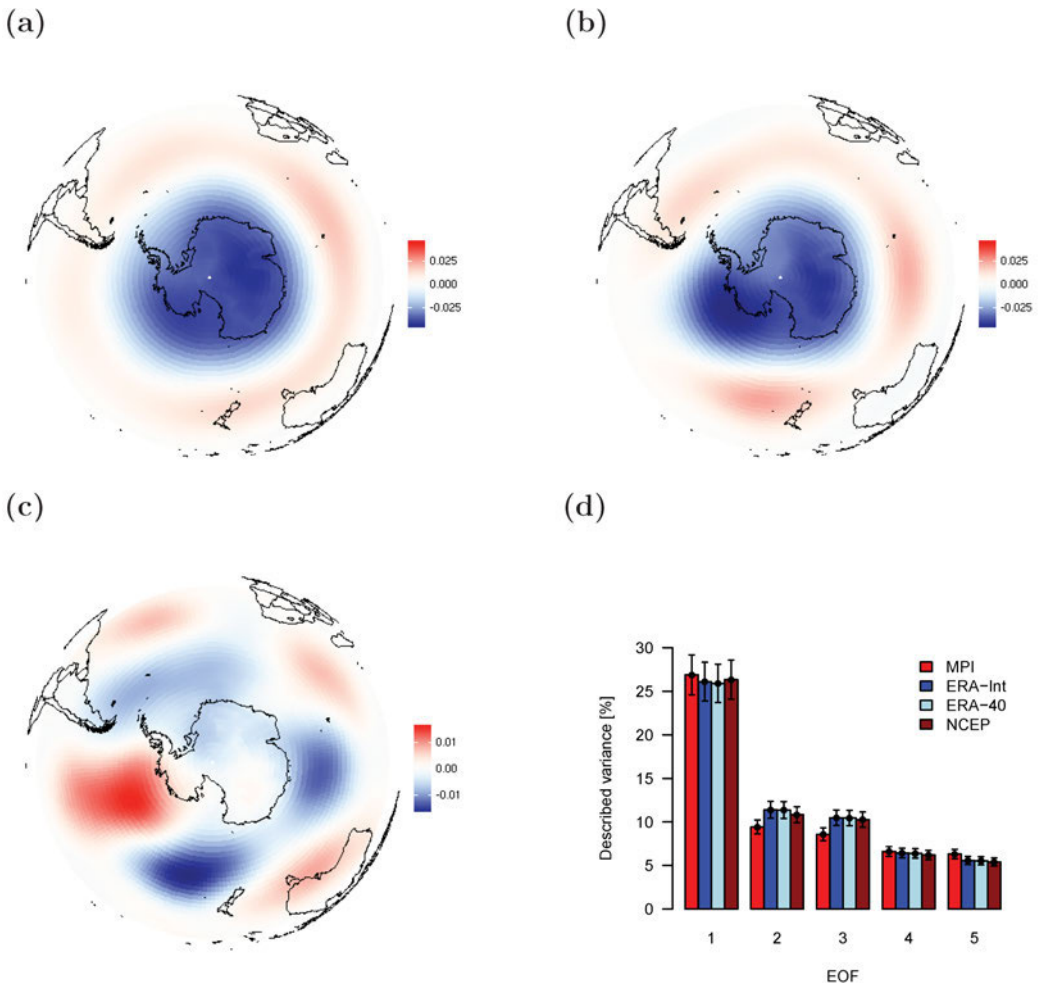

Figure 1: First EOF of Z_{700} anomalies from (a) MPI-ESM and (b) ERA-Interim reanalysis for the period 1979–2001. (c) Difference plot of the first EOFs of MPI-ESM and ERA-Interim: $EOF1_{MPI\text{-}ESM}$ (shown in (a) and (b)) for the Z_{700} field and the same period. (d) Proportion of the total variance [%] associated with the first 5 EOFs for MPI-ESM model and ERA-Interim, ERA-40, and NCEP/NCAR reanalyses. Errorbars are estimates of sampling errors in EOF computation according to "North's rule of thumb" (North et al., 1982).

ways: either parametrically, using auto-regressive processes of order p (AR[p]) or non-parametrically using kernel smoothing (e.g., Priestley, 1992; Venables and Ripley, 2002). We use AR[p] processes with the Yule-Walker-equations to estimate the associated parameters (e.g., Brockwell and Davis, 1991; Box and Jenkins, 1976); the Akaike-Information Criterion (AIC, e.g. deLeeuw, 1992; Venables and Ripley, 2002) guides the selection of orders p. Additionally, a modified Daniell kernel is used as a non-parametric density estimate with the degree of smoothness defined such that it roughly corresponds to the flexibility of the associated AR-process. Spectral density estimates are based on the R-functions `spec.pgram()` and `spec.ar()` (R Core Team, 2013).

2.5 Composite and correlation analysis

Composites for months with an anomalous high or low AAO index are the basis for investigating the potential mechanisms associated with rainfall over the southern hemisphere. Monthly values exceeding (undercutting) the calculated and normalised AAO index 1979–2001 mean about plus (minus) one standard deviation (Hendon et al., 2007) were averaged and defined as positive (negative) composite. Afterwards the 1979–2001 mean monthly precipitation was removed from composites, respectively. Spearman's rank correlation coefficient quantifies the relationship between the AAO index time series and the series of monthly precipitation means (Wilks, 2011).

3 Results

3.1 Spatial variabililty patterns

The leading spatial patterns of variability (first EOFs) for Z_{700} anomalies (Figure 1(a),(b)) account for roughly 26 % of the total variability for the MPI-ESM, for the three reanalyses (Figure 1(d)) the portion of variability is slightly lower. The subsequent EOFs represent about 10 % and less of the total variability; here the 2nd and

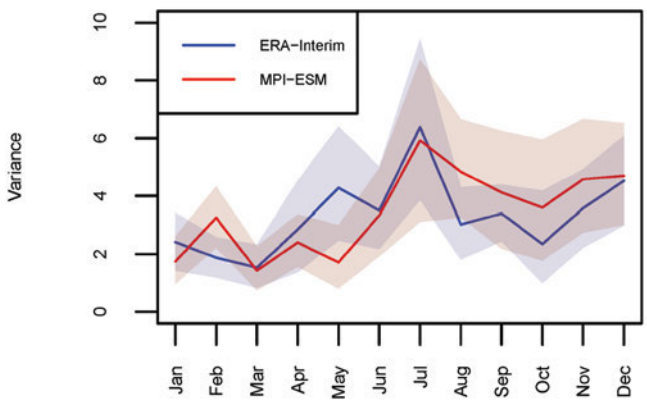

Figure 2: Variances of monthly mean AAO index for MPI-ESM (red solid line) and ERA-Interim (blue solid line) for the 1979–2001 period. The shading depicts a 95 % confidence interval for monthly mean variances.

3rd EOF associated with the MPI-ESM represent slightly less variability than their counterparts from the reanalyses and thus compensating for the larger portion associated to the first EOF (Figure 1(d)).

Figure 1(a) and (b) show the spatial patterns for MPI-ESM and ERA-Interim, respectively. Both show a strong zonal symmetry resulting in an almost concentrical structure around the South Pole. This pattern is known as the positive phase of the Antarctic Oscillation pattern (Thompson and Wallace, 2000). The typical three centres of action (Mo, 2000) in the southern oceans break the circular symmetry and lie along 40° S, located at about 90° E, 50° W, and 170° W and are readily visible for the AAO pattern obtained for ERA-Interim (Figure 1(b)). The MPI-ESM shows a stronger circular symmetry and consequently these three centres are less pronounced. Furthermore, a slight shift compared to the reanalysis becomes evident in a difference plot in Figure 1(c). The centres in the Pacific sector (170° W) and Indian sector (90° E) are shifted anti-clockwise. The difference pattern of the leading EOFs of the reanalysis and the MPI-ESM-MR shows four prominent features, Figure 1: a strong positive signal over the Bellingshausen and Amundsen Sea, a slight negative signal over the Weddell Sea, and two negative regions over the Ross Sea and the southern Indian Ocean. Jungclaus et al. (2013) also identified the first two features and reported a too strong low-pressure system in the Amundsen Sea region and significant differences in air-pressure distribution over the Weddell Sea. These two regions correspond to the location of the Antarctic Dipole (Yuan, 2004, and references therein); this dipole coins the reanalysis AAO pattern but is not a prominent feature of the MPI-ESM-MR's AAO pattern. However, the characteristic signature of this dipole can be found in MPI-ESM-MR's EOF2 (not shown). Thus, the model is in principle able to reproduce the dipole's pattern but not with 1) a comparable amplitude and 2) the proper connection to the models's AAO.

3.2 Seasonal cycle of AAO index variability

The annual cycle in the variability (variance) of the AAO index time series (first PC) peaks in the cold season (JJA). Figure 2 shows the annual cycle obtained for ERA-Interim (blue solid line) with 95 % confidence intervals (blue shading).

The MPI-ESM (red solid line and shading) reproduces this cycle to a large extent. Discrepancies are particularly present in May where the MPI-ESM shows lower variance, followed by a steeper increase in June and July. The subsequent decay of variability in August, September and October is slower for the MPI-ESM than for ERA-Interim. However, confidence intervals largely overlap and differences are likely to be not statistically significant on a reasonable level (i.e., $p \not< 0.05$).

3.3 Spectral Density of PCs

Figure 3 compares spectral density estimates for the first PC of ERA-Interim (light and dark blue) and MPI-ESM (light and dark red).

To give an impression of the uncertainty, the dotted line in the background shows the (unsmoothed) Fourier-periodogram of the first PC derived for ERA-Interim. A description with AR-processes of order $p = 1, \ldots, 15$ yields a smallest value for the AIC-value at $p = 1$, closely followed by $p = 6$ and $p = 7$. The result is highly similar for NCEP/NCAR and ERA-40 (not shown), however here the AIC prefers larger orders $p = 6$ and $p = 7$ over $p = 1$. As it is difficult to discriminate between the low order $p = 1$ and the larger orders $p = 6$ and $p = 7$ for the given reanalysis data sets, Figure 3 gives the spectral densities for orders $p = 1$ (solid lines, dark colours) and $p = 7$ (solid lines, light colours) for ERA-Interim (light and dark blue) and MPI-ESM (light and dark red). Note that a corresponding order selection with AIC for the MPI-ESM yields order $p = 1$; here higher orders (e.g., $p = 6$ or $p = 7$) are not as compatible with $p = 1$ as it is the case for the reanalyses.

Irrespective of the ambiguity of orders, the variability associated with frequencies larger than $f = 2/12$ (two months) is underrepresented in the MPI-ESM. The higher order AR-process (AR[7], or low degree of smoothing) suggests that particularly the variability at frequencies between $f = 4/12$ and $f = 5/12$, i.e. at periods of 4 to 5 months is underrepresented.

3.4 Link to Southern Hemispheric Precipitation

Table 2 gives the counts of anomalously high and low AAO index values (larger/smaller one standard deviation with reference to the 1979–2001 mean).

The months with positive (AAO^+) and negative (AAO^-) indices define positive (Figure 4 (a), (c)) and negative (Figure 4 (b), (d)) composites of precipitation anomalies for MPI-ESM and ERA-Interim, respectively.

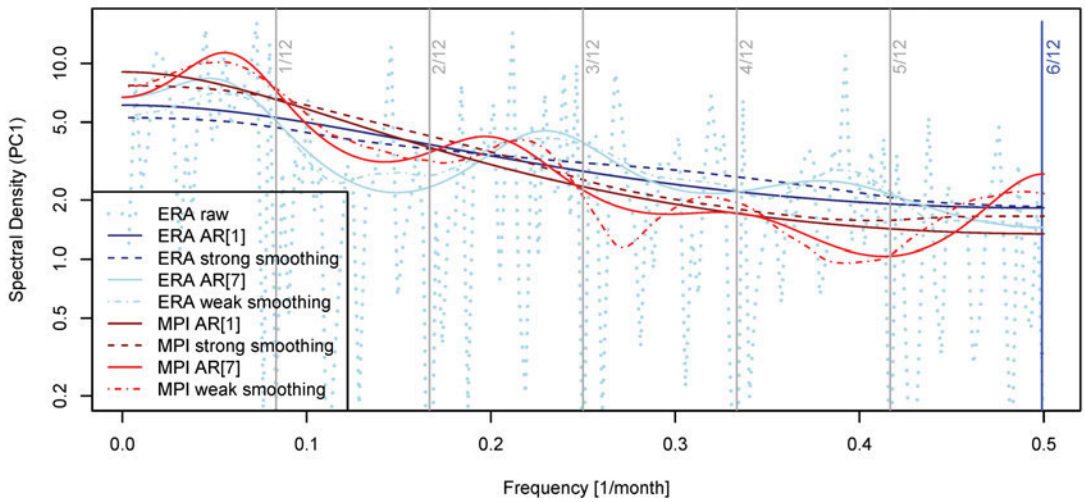

Figure 3: Spectral density estimates for the first PC obtained from ERA-Interim (light blue and dark blue) and MPI-ESM (light red and dark red). Solid lines show density estimates based on AR[1] (dark) and AR[7] (light); dashed lines give estimates based on smoothing with a modified Daniell kernel with high (dark colours) and low degree of smoothing (light colours). The light blue dotted line depicts the associated unsmoothed Fourier periodogram for ERA-Interim. The vertical lines mark the frequency of the annual cycle and higher harmonics $f = k/12, k = 1, \ldots, 6$.

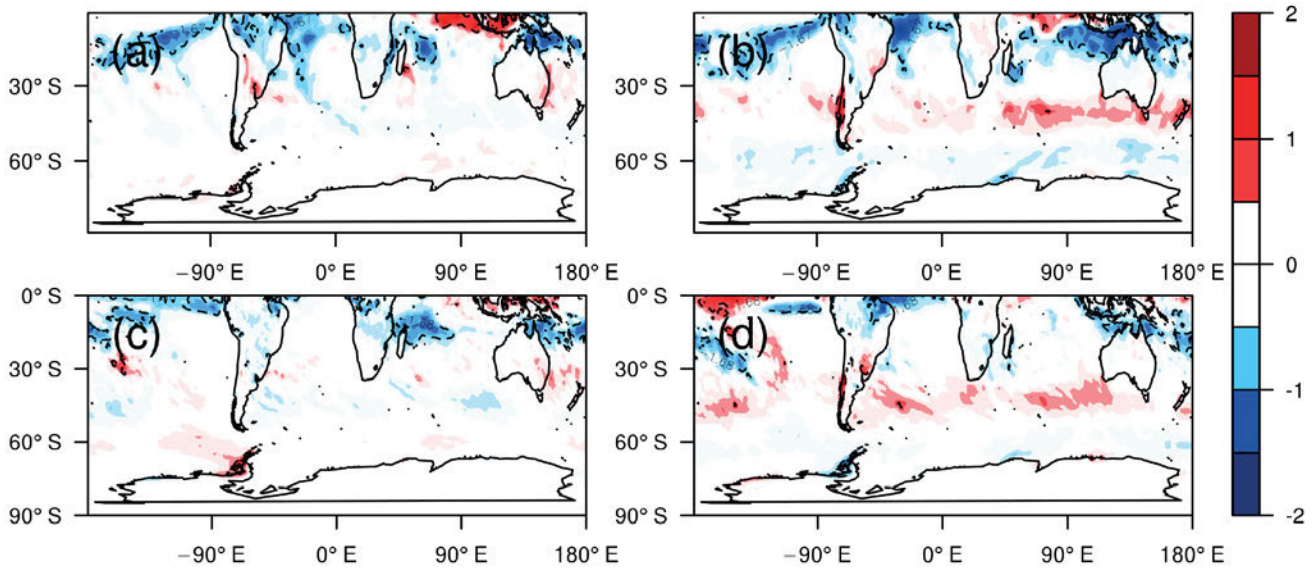

Figure 4: Composite anomalies (w.r.t. 1979–2001 mean) of monthly precipitation [mm per day]: (a) MPI-ESM during positive phases and (b) negative phases of the model AAO; (c) ERA-Interim reanalysis for positive phases and (d) negative phases. The dotted lines depict the 95 % confidence interval, respectively.

Table 2: Counts of monthly AAO indices exceeding (AAO^+) or undercutting (AAO^-) the 1979–2001 mean value about one standard deviation, respectively.

Model/Data	AAO^-	AAO^+
NCEP/NCAR	45	41
ERA-40	42	44
ERA-Interim	45	46
MPI-ESM	46	47

Both model and reanalysis composites suggest that negative AAO phases are associated with a band of precipitation increase in the midlatitudes (30° S – 50° S) and dryer conditions south of 50° S (Figure 4 (b), (d)). This "wet band" disappears for positive AAO phases (Figure 4 (a), (c)). During these phases the MPI-ESM overestimates precipitation anomalies in the Indonesian region and underestimates precipitation over the Antarctic Peninsula.

The model does recover ERA-Interim's spatial precipitation pattern during negative phases quite well. However, the MPI-ESM overestimates rainfall anomalies over a region around Western Indonesia and the "wet

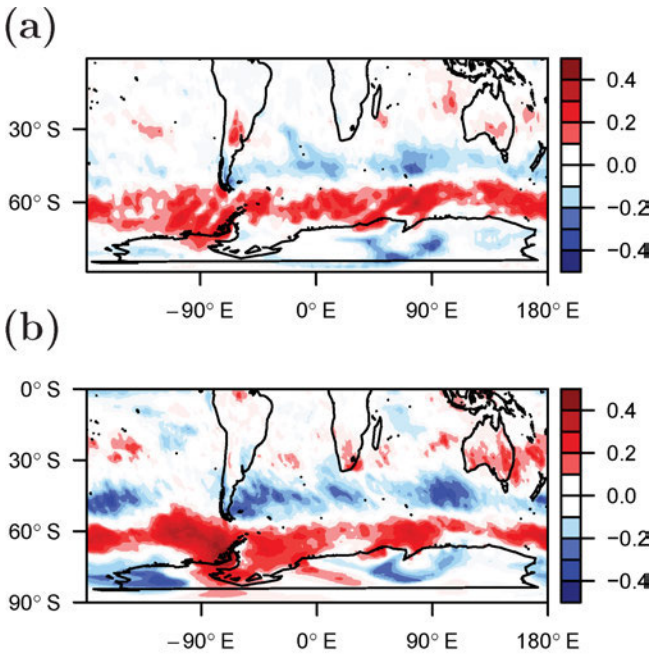

Figure 5: Spearman correlation coefficient between monthly precipitation means and the AAO index time series of (a) MPI-ESM and (b) ERA-Interim for the period 1979–2001. White indicates correlation being compatible with 0 at a 5 % level of significance.

band" of precipitation is less pronounced in the central South Atlantic and the central South Pacific (Figure 4 (b), (d)).

Additionally to positive/negative AAO composites, Figure 5 shows maps of the Spearman rank correlation coefficient estimated for the AAO index time series and monthly precipitation.

The strong zonal pattern of significant negative correlation between 40° S and 50° S in Figure 5(a) fits well with the "wet band" identified in Figure 4(b) for negative AAO phases. Positive correlation dominates the midlatitudes to polar regions in both model and reanalyses (NCEP/NCAR, ERA-40, not shown) and indicates an increase in precipitation here for positive phases. Discrepancies are most dominant in the Weddell Sea: positive correlation is weaker in the model which is associated with negative rainfall anomalies for a negative AAO index. van den Broeke and van Lipzig (2004) found that the western Antarctic Peninsula becomes drier when the AAO index is low; hence implying a positive correlation between precipitation and the index time series. As the correlation is reduced here for MPI-ESM, this mechanism is not as prominent in the model as in reanalyses. A lack of negative correlation over Marie Byrd Land (West Antarctica) and the adjacent Ross Sea is found for the MPI-ESM. The source of this asymmetric response in precipitation is determined by the direction of flow anomalies with respect to the Antarctic topography (van den Broeke and van Lipzig, 2004). Overall, the correlation is less pronounced (positive and negative) which indicates a weaker link between AAO and precipitation in the model.

4 Summary and discussion

We investigate to what extent the Antarctic Oscillation (AAO/SAM) is represented in the MPI Earth System Model (MPI-ESM-MR-hist) by comparing to three reanalyses (NCEP/NCAR, ERA-40, ERA-Interim). The leading EOF of monthly mean 700 hPa geopotential height anomalies defines the mode's spatial pattern and the associated PC defines the index time series. The leading EOF describes 27 % (MPI-ESM) and 26 % (ERA-Interim) of the total variance of the geopotential height anomaly field. The spatial patterns are roughly circular (zonally symmetric) due to landmass distribution in the southern hemisphere. The AAO's characteristic three centres of action are less pronounced in the MPI-ESM-MR and slightly shifted (Mo, 2000).

The differences pattern of the first EOFs shows distinct features over the Amundsen Sea, the Weddell Sea (i.e., the Antarctic Dipole, ADP) and two regions with stronger differences over the Ross Sea and the southern Indian Ocean. This indicates that the variability of the geopotential height contrast in the reanalyses in these locations is not adequately reproduced in the MPI-ESM. As Yuan (2004) suggests that the ADP is influenced by ENSO, a hypothesis about deficits in MPI-ESM-MR's ENSO simulation emerges and this might be responsible for part of the difference in the AAO patterns. Jungclaus et al. (2013) reports that MPI-ESM-MR is superior in ENSO modelling compared to the CMIP3 version of the MPI model but does not reproduce the appropriate seasonal modulation of the ENSO strength and neither the right ratio of El Niño and La Niña events. Thus improving these ENSO deficits might improve also MPI-ESM-MR's AAO characteristics.

For the absence of variability over the Ross Sea and the southern Indian Ocean a hypothesis connected to the ADP can be formulated: The centres of action are less pronounced (if at all present) in the model, geopotential height anomalies are either not so pronounced and/or are not associated with a fixed location. This can be thought as a consequence of the wave-3-pattern (Mo, 2000) being rather a progressing than a standing wave in the MPI-ESM. A propagating wave does not coin the stationary variability pattern (EOF1) as the standing wave in the ERA-Interim does. We expect furthermore the well pronounced ADP in the reanalyses to favour a standing wave-3-pattern. Consequently, we expect the same mechanisms responsible for a weak ADP in the MPI-ESM-MR leading also to the observed differences over the Ross Sea and the southern Indian Ocean.

The characteristic annual cycle of AAO index variability with the characteristic peak in the cold season is well reproduced by the MPI-ESM. A spectral analysis of the index time series reveals a lack of variability in the intra-seasonal range (periods of 4 to 5 months).

We furthermore assess the relation between the AAO and precipitation over the southern hemisphere through composites for negative and positive AAO phases and a correlation analysis. An increasing (decreasing) AAO

index implies an increasing (decreasing) equatorward directed meridional pressure gradient with poleward (equatorward) shifted westerlies and an extension (contraction) of the mean midlatitude storm track (Thompson and Wallace, 2000). The northward shift of westerlies causes increased precipitation between 30° to 50° S; this "wet band" of precipitation disappears for high AAO indices. The MPI-ESM underestimates precipitation during positive AAO phases over the Antarctic Peninsula and overestimates precipitation anomalies in the Indonesian region. Underestimation of precipitation over the peninsula could result from reduced air-pressure over the Amundsen sea in MPI-ESM via changes in the circulation and related precipitation.

Correlation plots quantify the link between the monthly AAO time series and southern hemispheric precipitation: the reanalysis correlation maps are to a large extent reproduced by the model. However, over southern Australia, the Weddell Sea, and the Antarctic Peninsula the MPI-ESM underestimates the strong link between AAO and precipitation. The missing dipolar-like structure in the correlation pattern between Weddell Sea and Antarctic Peninsula on the one hand and Amundsen Sea and West Antarctica on the other hand in the reanalysis is explained by the already mentioned underestimation of the low pressure system over Amundsen Sea. The prominent (surface) Amundsen Sea Low (ASL) is one of three climatological low pressure centres around Antarctica. In climatological mean the ASL contributes wet and warm (cold) air to the eastern (western) part of Antarctic peninsula. This mechanism is less distinct in the model and therefore accounts for missing positive and negative precipitation correlation in the west Antarctic area.

In conclusion the MPI-ESM in MR mode is in general able to reproduce central features of the AAO and related precipitation as found in the reanalyses, i.e. the dominant mode of atmospheric variability in the southern hemisphere is roughly captured. The models exaggerated zonal symmetry and the slight shift of the centres of action in the first EOF might result from the model's difficulties in reproducing properly the ENSO characteristics. It might be related to differences in precipitation distribution.

References

Berman, A., G. Silvestri, R. Compagnucci, 2012: Eastern patagonia seasonal precipitation: influence of Southern Hemisphere circulation and links with subtropical South American precipitation. – J. Climate **25**, 6781–6795.

Berman, A., G. Silvestri, R. Compagnucci, 2013: On the variability of seasonal temperature in southern South America. – Climate Dyn. **40**, 1863–1878.

Box, G.E.P., G.M. Jenkins, 1976: Time Series Analysis: Forecasting and Control. – Prentice Hall, New Jersey.

Brockwell, P.J., R.A. Davis, 1991: Time series: Theory and Methods Springer Series in Statistics. – Springer, Berlin.

Carvalho, L., C. Jones, T. Ambrizzi, 2005: Opposite phases of the Antarctic Oscillation and relationships with intraseasonal to interannual activity in the tropics during the austral summer. – J. Climate **18**, 702–718.

Climate Prediction Center, 2014: Website. – Available online at www.cpc.noaa.gov; visited on March 8th 2014.

Dee, D.P., S.M. Uppala, A.J. Simmons, P. Berrisford, P. Poli, S. Kobayashi, U. Andrae, M.A. Balmaseda, G. Balsamo, P. Bauer, P. Bechtold, A.C.M. Beljaars, L. van de Berg, J. Bidlot, N. Bormann, C. Delsol, R. Dragani, M. Fuentes, A.J. Geer, L. Haimberger, S. Healy, H. Hersbach, E.V. Holm, L. Isaksen, P. Kållberg, M. Koehler, M. Matricardi, A.P. McNally, B.M. Monge Sanz, J.-J.Morcrette, B.-K. Park, C. Peubey, P. de Rosnay, C. Tavolato, J.-N. Thepaut, F. Vitart, 2011: The ERA-Interim reanalysis: configuration and performance of the data assimilation system. – Quart. J. Roy. Meteor. Soc. **137**, 553–597.

deLeeuw, J., 1992: Akaike (1973) information theory and an extension of the maximum likelihood principle. – In: S. Kotz, N.L. Johnson (Eds.): Breakthroughs in Statistics, volume 1. – Springer, London, 599–609.

Gillett, N., T. Kell, P. Jones, 2006: Regional climate impacts of the Southern Annular Mode. – Geophys. Res. Lett. **33**, L23704.

Giorgetta, M.A., J. Jungclaus, C.H. Reick, S. Legutke, J. Bader, M. Böttinger, V. Brovkin, T. Crueger, M. Esch, K. Fieg, K. Glushak, V. Gayler, H. Haak, H.-D. Hollweg, T. Ilyina, S. Kinne, L. Kornblueh, D. Matei, T. Mauritsen, U. Mikolajewicz, W. Mueller, D. Notz, F. Pithan, T. Raddatz, S. Rast, R. Redler, E. Roeckner, H. Schmidt, R. Schnur, J. Segschneider, K.D. Six, M. Stockhause, C. Timmreck, J. Wegner, H. Widmann, K.-H. Wieners, M. Claussen, J. Marotzke, B. Stevens, 2013: Climate and carbon cycle changes from 1850 to 2100 in MPI-ESM simulations for the Coupled Model Intercomparison Project phase 5. – J. Adv. Model. Earth Syst. **5**, 572–597.

Hannachi, A., I.T. Jolliffe, D.B. Stephenson, 2007: Empirical orthogonal functions and related techniques in atmospheric science: A review. – Int. J. Climatol. **27**, 1119–1152.

Hendon, H.H., D.W.J. Thompson, M.C. Wheeler, 2007: Australian Rainfall and Surface Temperature Variations Associated with the Southern Hemisphere Annular Mode. – J. Climate **20**, 2452–2467.

Ilyina, T., K.D. Six, J. Segschneider, E. Maier-Reimer, H. Li, I. Núñez-Riboni, 2013: Global ocean biogeochemistry model HAMOCC: Model architecture and performance as component of the MPI-Earth system model in different CMIP5 experimental realizations. – J. Adv. Model. Earth Syst. **5**, 287–315.

Jolliffe, I.T., 2002: Principal Component Analysis Springer Series in Statistics. – Springer, New York, 489.

Jungclaus, J.H., N. Fischer, H. Haak, K. Lohmann, J. Marotzke, D. Matei, U. Mikolajewicz, D. Notz, J.S. von Storch, 2013: Characteristics of the ocean simulations in the Max Planck Institute Ocean Model (MPIOM) the ocean component of the MPI-Earth system model. – J. Adv. Model. Earth Syst. **5**, 422–446.

Kalnay, E., M. Kanamitsu, R. Kistler, 1996: The NCEP/NCAR 40-Year Reanalysis Project. – Bull. Amer. Meteor. Soc. **77**, 437–471.

Kidson, J.W., 1988: Indices of the Southern Hemisphere Zonal Wind. – J. Climate **1**, 183–194.

Kidson, J.W., 1999: Principal Modes of Southern Hemisphere low-frequency variability obtained from NCEP-NCAR reanalyses. – J. Climate **12**, 2808–2830.

Kistler, R., E.M. Kalnay, W. Collins, 2001: The NCEP/NCAR 50-Year Reanalysis: Monthly Means CD-

ROM and documentation. – Bull. Amer. Meteor. Soc. **82**, 247–268.

Kruschke, T., H.W. Rust, C. Kadow, G. Leckebusch, U. Ulbrich, 2014: Evaluating decadal predictions of northern hemispheric cyclone frequencies. – Tellus A **66**, 22830.

Kruschke, T., H.W. Rust, C. Kadow, W. Müller, H. Pohlmann, G. Leckebusch, U. Ulbrich, 2016: Probabilistic evaluation of decadal predictions for northern hemisphere winter storms. – Meteorol. Z. **this issue**.

Marotzke, J., W.A. Mueller, F.S.E. Vamborg, P. Becker, U. Cubasch, H. Feldmann, F. Kaspar, C. Kottmeier, C. Marini, I. Polkova, K. Prömmel, H.W. Rust, D. Stammer, U. Ulbrich, C. Kadow, A. Köhl, J. Kröger, T. Kruschke, J.G. Pinto, H. Pohlmann, M. Reyers, M. Schröder, F. Sienz, C. Timmreck, M. Ziese, 2016: MiKlip - a National Research Project on Decadal Climate Prediction. – Bull. Amer. Meteor. Soc., published online. DOI: 10.1175/BAMS-D-15-00184.1.

Marsland, S.J., H. Haak, J.H. Jungclaus, M. Latif, F. Roeske, 2003: The Max-Planck-Institute global ocean/sea-ice model with orthogonal curvilinear coordinates. – Ocean Modelling **5**, 91–127.

Meneghini, B., I. Simmonds, I. Smith, 2007: Association between Australian rainfall and the Southern Annular Mode. – Int. J. Climatol. **27**, 109–121.

Mo, K.C., 2000: Relationships between Low-Frequency Variability in the Southern Hemisphere and Sea Surface Temperature Anomalies. – J. Climate **13**, 3599–3610.

Moy, C.M., P.I. Moreno, R.B. Dunbar, M.R. Kaplan, J.-P. Francois, R. Villalba, T. Haberzettl, 2009: Climate Change in Southern South America During the Last Two Millennia. – In: F. Vimeux, F. Sylvestre, M. Khodri (Eds.): Past Climate Variability in South America and Surrounding Regions. Developments in Paleoenvironmental Research **14**. – Springer Netherlands, 353–393.

Müller, W., J. Baehr, H. Haak, J. Jungclaus, J. Kröger, D. Matei, D. Notz, H. Pohlmann, J. von Storch, J. Marotzke, 2012: Forecast skill of multi-year seasonal means in the decadal prediction system of the Max Planck Institute for Meteorology. – Geophys. Res. Lett. **39**, L22707.

North, G.R., T.L. Bell, R.F. Cahalan, F.J. Moeng, 1982: Sampling errors in the estimation of empirical orthogonal functions. – Mon. Wea. Rev. **110**, 699–706.

Pezza, L.B., T. Durrant, I. Simmonds, I. Smith, 2008: Southern Hemisphere Synoptic Behavior in Extreme Phases of SAM, ENSO, Sea Ice Extent, and Southern Australia Rainfall. – J. Climate **21**, 5566–5584.

Pohlmann, H., W.A. Müller, K. Kulkarni, M. Kameswarrao, D. Matei, F.S.E. Vamborg, C. Kadow, S. Illing, J. Marotzke, 2013: Improved forecast skill in the tropics in the new MiKlip decadal climate predictions. – Geophys. Res. Lett. **40**, 5798–5802.

Priestley, M.B., 1992: Spectral Analysis and Time Series. – Academic Press, London.

R Core Team, 2013: R: A Language and Environment for Statistical Computing. – R Foundation for Statistical Computing, Vienna, Austria.

Raddatz, T.J., C.H. Reick, W. Knorr, J. Kattge, E. Roeckner, R. Schnur, K.G. Schnitzler, P. Wetzel, J.H. Jungclaus, 2007: Will the tropical landbiosphere dominate the climate-carbon cycle feedback during the twenty-first century?. – Climate Dyn. **29**, 565–574.

Rashid, H.A., I. Simmonds, 2005: Southern hemisphere annular mode variability and the role of optimal nonmodal growth. – J. Atmos. Sci. **62**, 1947–1961.

Reason, C.J.C., M. Rouault, 2005: Links between the Antarctic Oscillation and winter rainfall over western South Africa. – Geophys. Res. Lett. **32**, L07705, DOI: 10.1029/2005GL022419.

Renwick, J., D. Thompson, 2006: The Southern Annular Mode and New Zealand climate. – Water and Atmosphere **14**, 24–25.

Silvestri, G.E., C.S. Vera, 2003: Antarctic Oscillation signal on precipitation anomalies over southeastern South America. – Geophys. Res. Lett. **30**, 2115. DOI: 10.1029/2003GL018277.

Silvestri, G.E., C.S. Vera, 2009: Non-stationary impacts of the Southern Annular Mode on Southern Hemisphere climate. – J. Climate **22**, 6142–6148.

Stevens, B., M. Giorgetta, M. Esch, T. Mauritsen, T. Crueger, S. Rast, M. Salzmann, H. Schmidt, J. Bader, K. Block, R. Brokopf, I. Fast, S. Kinne, L. Kornblueh, U. Lohmann, R. Pincus, T. Reichler, E. Roeckner, 2013: Atmospheric component of the MPI-M Earth System Model: ECHAM6. – J. Adv. Model. Earth Syst. **5**, 146–172.

Taylor, K.E., R.J. Stouffer, G.A. Meehl, 2012: An overview of CMIP5 and the experiment design. – Bull. Amer. Meteor. Soc. **93**, 485–498.

Thompson, D., J.M. Wallace, 2000: Annular modes in the extratropical circulation. Part I: Month-to-month variability. – J. Climate **13**, 1000–1016.

Ummenhofer, C., M. England, 2007: Interannual extremes in New Zealand precipitation linked to modes of Southern Hemisphere climate variability. – J. Climate **20**, 5418–5440.

Uppala, S.M., P.W. Kållberg, A.J. Simmons, U. Andrae, da V. Costa Bechtold, M. Fiorino, J.K. Gibson, J. Haseler, A. Hernandez, G.A. Kelly, X. Li, K. Onogi, S. Saarinen, N. Sokka, R.P. Allan, E. Andersson, K. Arpe, M.A. Balmaseda, A.C.M. Beljaars, L. van de Berg, J. Bidlot, N. Bormann, S. Caires, F. Chevallier, A. Dethof, M. Dragosavac, M. Fisher, M. Fuentes, S. Hagemann, E. Holm, B.J. Hoskins, L. Isaksen, P.A.E.M. Janssen, R. Jenne, A.P. McNally, J.-F. Mahfouf, J.-J. Morcrette, N.A. Rayner, R.W. Saunders, P. Simon, A. Sterl, K.E. Trenberth, A. Untch, D. Vasiljevic, P. Viterbo,, J. Woollen, 2005: The ERA-40 re-analysis. – Quart. J. Roy. Meteor. Soc. **131**, 2961–3012.

Valcke, S., 2013: The OASIS3 coupler: a European climate modelling community software. – Geosci. Model Develop. **6**, 373–388.

van den Broeke, M.R., N.P.M. van Lipzig, 2004: Changes in Antarctic temperature, wind and precipitation in response to the Antarctic Oscillation. – Ann. Glaciol. **39**, 119–126.

Venables, W.N., B.D. Ripley, 2002: Modern Applied Statistics with S – Springer, New York.

Wilks, D.S., 2011: Statistical methods in the atmospheric sciences – Academic Press, San Diego, CA.

Yuan, X., 2004: Enso-related impacts on antarctic sea ice: a synthesis of phenomenon and mechanisms. – Antarctic Sci. **16**, 415–425.